Self-organised Lasers of Reconfigurable Colloidal Assemblies

Manish Trivedi,[1†] Dhruv Saxena,[2†] Wai Kit Ng,[2†] Riccardo Sapienza,[2*] Giorgio Volpe[1*]

[1]Department of Chemistry, University College London, 20 Gordon Street,
London WC1H 0AJ, United Kingdom
[2]The Blackett Laboratory, Department of Physics,
Imperial College London, London SW7 2BW, United Kingdom

[†]These authors contributed equally
[*]To whom correspondence should be addressed; E-mail: r.sapienza@imperial.ac.uk; g.volpe@ucl.ac.uk

Abstract

Non-equilibrium assemblies, where units are able to harness available energy to perform tasks, can often self-organise into dynamic materials that uniquely blend structure with functionality and responsiveness to their environment. The integration of similar features in photonic materials remains challenging, yet desirable in order to manufacture active, adaptive and autonomous photonic devices. Here we show the self-organisation of programmable random lasers from the reversible out-of-equilibrium self-assembly of colloids. Random lasing originates from the optical amplification of light undergoing multiple scattering within the dissipative colloidal assemblies and therefore depends crucially on their self-organisation behaviour. Under external light stimuli, these dynamic random lasers are responsive and present a continuously tuneable laser threshold. They can therefore reconfigure and cooperate by emulating the ever-evolving spatiotemporal relationship between structure and functionality that is typical of many non-equilibrium assemblies.

Main text

Self-organisation is the spontaneous emergence of structure and coordination from elementary units on larger scales than those defining the individual components [1]. Many biological and artificial systems capable of harnessing available energy rely on this process to form complex structures and patterns as well as to achieve complex functionalities [2, 3]. Inspired by their biological counterpart, the goal of controlling artificial non-equilibrium systems to self-assemble into reconfigurable, adaptive and autonomous artificial materials has driven a particularly vast scientific effort [4, 5, 6, 7, 8, 9]. In colloidal science, colloidal systems that can engage in dissipative self-assembly after energy conversion have come to the fore due to their ability, e.g., to emulate biological self-organisation [10, 11, 12, 13], to transport and reversibly assemble passive colloidal cargoes [14, 15, 16, 17], and to implement microscopic metamachines and mechanical devices [18, 19, 20].

Because of the ease of synthesis with sizes comparable to the wavelengths of visible light, colloids have often been the building blocks of choice for photonic materials and devices with optical properties defined by their fixed topology and spatial correlations [21, 22]. Adding optical gain to these static photonic assemblies can trigger lasing [23]. In disordered assemblies, random lasing [24, 23] has been observed in solid photonic glasses [25], titania ($\mathrm{TiO_2}$) colloidal systems [26], semiconductor powders [27], and more complex geometries [28, 29]. These lasing functionalities emerging in the final assembled photonic materials are reaching technological applications (from low-coherence imaging [30] to super-resolution spectroscopy [31], from sensing [32] to even interfacing with living tissues [33]), thanks to the flexibility and shape insensitivity of random lasing processes.

Reconfigurable photonic architectures, capable of actively controlling light flow, are sought after for the implementation of next-generation photonic devices [34], and reconfigurable lasers, whose lasing action can be controlled post-fabrication, are an emerging concept still in its infancy [35]. Random lasers fabricated from colloidal assemblies are indeed locked in their final configuration, thus proposing optical functionalities which are overwhelmingly static and fixed. Here we realise programmable random lasers, which self-organise from the dissipative self-assembly of colloids after light absorption from a few units and show dynamic features, such as responsiveness, reconfigurability and cooperation. Lasing emerges when the colloidal cluster dynamically reaches a threshold size which is controlled by the self-assembly process.

Colloids in solutions of laser dyes can scatter and amplify light that is trapped within them. When optically pumped by a high-energy laser of constant spot size and intensity (Methods), lasing can emerge when the local colloidal density increases above a threshold such that light travels an average optical path long enough for net amplification to occur before leaving the medium. This is the onset of random lasing [23] reached by increased scattering. In Fig. 1a-b, we drive the self-assembly of freely diffusing polyethylenimine-functionalised monodisperse $\mathrm{TiO_2}$ colloids of radius $R_{\mathrm{TiO_2}} = 0.915 \pm 0.03\,\mu\mathrm{m}$ (Figs. E1-E2) in an ethanol solution of a rhodamine-based dye (rhodamine 6G or B) by generating a local temperature gradient around a carbon-coated Janus particle ($R_{\mathrm{S}} = 4.22 \pm 0.14\,\mu\mathrm{m}$) (Methods). By exploiting different

mechanisms including, e.g., convection, thermophoresis, thermo-osmosis, thermo-electricity and depletion effects [36, 37, 38, 39, 40, 41], light-induced temperature gradients are indeed well-versed to manipulate colloidal particles and have found extensive use for optofluidic applications [42]. Under illumination by a continuous-wave 632.8 nm HeNe laser (Fig. E3) (Methods), the Janus particle heats up because of light absorption, a $\mathrm{TiO_2}$ colloidal cluster assembles around it (Fig. 1b), and the particle assumes a cap-down orientation due to its equilibrium rotational dynamics (Fig. E4). On removal of the external energy source, the colloids disperse reversibly (Fig. 1c). The process of dissipative gathering can then be reiterated, leading to re-accumulation of colloids around the Janus particle (Fig. E5). As soon as a dense cluster is formed (Fig. 1b), lasing action can emerge dynamically via this phenomenon of dissipative self-organisation. The lasing process is quantifiable by instantaneously measuring the emission spectra at different stages of this process (Fig. 1d) by pumping optically with a 532 nm pulsed laser (400 ps duration) at increasing pump fluence (Fig. E3) (Methods). The lasing threshold is reached when the linewidth of the emission spectrum narrows to 13.5 nm, i.e. half of its initial value (Fig. 1e-f). Lasing emission is generated by optical modes extending in the plane containing the colloids and we detect the light scattered in the out-of-plane direction. These spectra highlight the programmable optical functionality of these colloidal assemblies: lasing can be switched on/off dynamically by controlling the density and size of the cluster within the pump region (52 μm in diameter). The initial concentration of 2×10^{15} particles m^{-3} (Fig. 1a) is too low to obtain lasing, and we only observe the broad emission characteristic of the dye fluorescence. A significantly larger, higher-density (12×10^{15} particles m^{-3}) cluster as after accumulation and re-accumulation (Figs. 1b and E5), however, shows a single narrow peak at 560 nm with linewidth of $\sim$5 nm. During dispersal (Fig. 1c), the spectrum broadens again, thus evolving towards the initial fluorescence background. The power dependence evolution of the spectra in Fig. 1e-f indicates that the cluster is lasing at a threshold power of 70 mJ cm^{-2}, with two clear signatures of lasing [23]: a marked superlinear increase in the emission intensity and a significant reduction in spectral linewidth.

We can interpret and quantitatively reproduce the dissipative accumulation of colloids, which leads to crossing the lasing threshold, with a two-dimensional model based on thermal effects, where colloids in solution are drawn towards higher temperatures. Fig. 2a shows the calculated steady-state temperature profile around the heat source (the illuminated Janus particle), which approximately decays with the inverse of the radial distance r from the source (Methods). For the fixed HeNe laser intensity in our experiments (0.14 mW $\mu\mathrm{m}^{-2}$), we measured a temperature increase $\Delta T = 57 \pm 1.6\,^{\circ}\mathrm{C}$ over room temperature, corresponding to a source temperature $T_{\mathrm{s}} = 78 \pm 1.6\,^{\circ}\mathrm{C}$ (Fig. E6). This sharp radial thermal gradient produces a temperature-induced drift, which drags the $\mathrm{TiO_2}$ particles in the radial direction determined by their overall temperature-induced mobility μ_T. This parameter incorporates all the information about the interfacial interactions between the liquid and the solid that can be quite complex due to, e.g., thermo-osmotic, thermophoretic, thermo-electric or depletion contributions [42, 41].

The drift velocity of the colloids in the radial direction $\hat{\mathbf{e}}_r$ can then be defined as [42, 41]

$$\mathbf{u}(r) = -\mu_T \frac{\partial T(r)}{\partial r} \hat{\mathbf{e}}_r, \tag{1}$$

where $\mu_T \approx -1\,\mu\mathrm{m}^2\,\mathrm{K}^{-1}\,\mathrm{s}^{-1}$ is the only fitting parameter with the units of a thermo-diffusion coefficient extracted from our data (Fig. 2b). As $\mu_T < 0$, particles migrate towards warmer regions. Fig. 2b and the arrows in Fig. 2a show how the magnitude of $\mathbf{u}(r)$ increases, both in experiments and model, as $\sim r^{-2}$ when nearing the heat source, so that, as shown by the simulated trajectory in Fig. 2a (Methods), the motion of a single $\mathrm{TiO_2}$ particle becomes more directed with proximity to the source. The experimental dissipative dynamics of accumulation, dispersal and re-accumulation of the colloidal assembly can be thus well replicated with a simple two-dimensional particle-based model that includes this temperature-induced drive towards the heat source and a short range repulsive interaction among the colloids in the order of $\sim k_\mathrm{B}T$ (Fig. 2c) (Methods). The cluster rate of growth is steeper at the start of the process as colloids within a $\sim 4R_\mathrm{s}$ distance from the Janus particle experience stronger drifts ($\gtrsim 1\,\mu\,\mathrm{s}^{-1}$, Fig. 2b). As close-by colloids are quickly drawn towards the heat source, those that are farther away take longer to arrive as their motion is dominated by their Brownian dynamics (less directed) due to $\mathbf{u} \to \mathbf{0}$ as $\partial T/\partial r \to 0$ (i.e. for $r \to \infty$), thus the rate of accumulation of new colloids around the cluster slows down in time [43]. When the heat source is turned off, the assembly dissolves driven by diffusion and a short-ranged inter-particle repulsion with a rate of dispersal tending to zero as colloids evolve towards an equilibrium distribution (Fig. 2c) (Methods). When the heat source is back on, colloids re-accumulate much faster than in the first accumulation phase due to the now higher colloidal density around the heat source (Fig. 2c and E5).

Random lasing action occurs for a strongly enough scattering medium with a short enough scattering mean free path ℓ_sc and large enough excited cluster (as in Fig. 1b). This condition can be quantified by the critical radius R_cr, function of ℓ_sc, as lasing action can only be achieved if the excited random laser area is of radius $R_\mathrm{ex} > R_\mathrm{cr}$ [23]. For colloidal assemblies, R_cr can be calculated by solving the radiative-transfer equation for light (Methods). In our experiments, R_cr is a time-dependent variable as ℓ_sc changes in time due to the accumulation and dispersal of colloids. Fig. 2d reveals how R_cr decreases monotonically with increasing particle densities, thus facilitating the narrowing of the linewidth and lasing action. This trend is confirmed by the equivalent experimental data in Fig. 2e, where we determine R_cr dependence on particle density by pumping large colloidal assemblies with different $\mathrm{TiO_2}$ concentrations at a fixed pump fluence (140 mJ cm^{-2}) while varying the pump spot size (Methods). Based on Fig. 1e-f, R_cr is taken as the pump size where the linewidth of the emission spectrum narrows to half of its initial value, i.e. to 13.5 nm, in good agreement with model predictions (Fig. 2d), where the only fitting parameter is the net gain length (Methods). The particle densities before and after accumulation are marked on Fig. 2d showing that R_ex is smaller (larger) than R_cr before (after) accumulation, thus explaining why we observe lasing only after a certain accumulation time, i.e. for large enough assemblies (larger than R_cr), yet not before accumulation or after dissipation.

The dynamic nature of the dissipative self-organisation behind our random lasers, linking structure with optical functionality, can be harnessed to achieve unconventional tasks for standard random lasers, such as reconfigurability in space and time. Employing heat sources at different locations, lasing action can be triggered first and then transferred in space, thus shifting the lasing load within the sample. Fig. 3 shows how two Janus particles, placed approximately one pump spot size apart, alternatively act as accumulation points for the $\mathrm{TiO_2}$ colloids, when respectively activated by the external energy source. Lasing action is then switched from one heat source to the other by transferring the colloidal scattering load across, and back.

Janus particles can also cooperate to achieve feats beyond what achievable by a single particle. Fig. 4 shows how cooperation of properly located heat sources can lead to boosting the lasing properties and morph the laser spatially by imparting different shapes to the colloidal assemblies. While the colloidal assembly in Fig. 4a is too small to lase as $R_{\mathrm{ex}} < R_{\mathrm{cr}}$ (Fig. 4d), the addition of further colloids by a second Janus particle (Fig. 4b) pushes the cluster size just above the threshold for lasing ($R_{\mathrm{ex}} \approx R_{\mathrm{cr}}$ in Fig. 4d). This effect becomes even more pronounced when a third Janus particle joins the assembly as $R_{\mathrm{ex}} > R_{\mathrm{cr}}$ (Fig. 4c-d). Beyond the possibility of refining the laser spectral properties, another alluring application for multiple cooperating Janus particles is the possibility to define different planar laser geometries (Fig. 4e), which could be important for display applications, for travelling through narrow channels, or for adhering to complexly shaped targets.

In conclusion, we have performed the first experimental demonstration of an artificial colloidal material that, by virtue of dissipative self-assembly dynamics, can spontaneously self-organise in a random laser device, which dynamically blends morphology with its optical functionality. By reversibly accumulating colloids with temperature gradients, we enable an advanced photonic application (i.e. lasing), when, previously, particle motion in thermal gradients had only been used to inhibit lasing [44]. While here we employed Janus particles as heat sources to control the colloidal self-assembly dynamics, our results can be generalised to alternative light-absorbing materials (e.g. other gold-based and carbon-based materials or dye-doped beads) as well as to direct light absorption by the solvent, provided that these alternative approaches do not interfere with laser action (e.g. by causing dye bleaching effects). These self-organised random lasers can be manipulated on demand to produce controllable and programmable lasing, thus bringing novel functionalities to the field of photonics and opening the door for a new class of active functional materials in active matter. Due to the efficient gain medium and strong light trapping properties, these lasers have a relatively small size (a few tens of μm), which can be beneficial for applications requiring small footprints, including the realisation of display pixels, high-brightness light sources for low-coherence illumination, sensors for microfluidics and signal multiplexers [35]. While the lasers demonstrated here are quasi-two-dimensional and require minutes to reconfigure, two-dimensional and three-dimensional random lasers with faster responses (yet slower than electronic switching) can be achieved by, e.g., exploiting additional or alternative stimuli to thermal gradients, such as optical or electric fields [45, 46] to find application in, e.g., e-ink displays. Ultimately, the responsiveness, reconfigurability and cooperation properties of our self-organised lasers are a first step towards the

realisation of fully animate lasers capable of independent motion and autonomous adaptation in response to external stimuli [4]. Indeed, we envisage that the realisation of similar self-organised lasers from light-actuated colloidal molecules [16, 17] will pave the way towards the development of a new class of functional materials with potential for sensing applications [47], non-conventional computing [48], novel light sources, speckle-free illumination [30] and display technology [49].

Acknowledgements

We are grateful to Samantha Rueber, Matthew Blunt and Valentino Barbieri for initial training on experimental techniques. GV acknowledges sponsorship for this work by the US Office of Naval Research Global (Award No. N62909-18-1-2170). WKN acknowledges the research support funded by the President's PhD Scholarships from Imperial College London. RS and DS acknowledges support from The Engineering and Physical Sciences Research Council (EPSRC), grant number EP/T027258, and the European Community.

Author Contributions Statement

Author contributions are defined based on the CRediT (Contributor Roles Taxonomy) and listed alphabetically. Conceptualisation: RS, GV. Data Curation: WKN, MT. Formal analysis: WKN, DS, MT, GV. Funding acquisition: RS, GV. Investigation: WKN, RS, DS, MT, GV. Methodology: WKN, RS, MT, GV. Project administration: RS, DS, MT, GV. Software: WKN, DS, GV. Supervision: RS, GV. Validation: WKN, DS, MT. Visualisation: All. Writing – original draft: All. Writing – review and editing: All.

Competing Interests Statement

The authors have no competing interests.

Figure Captions

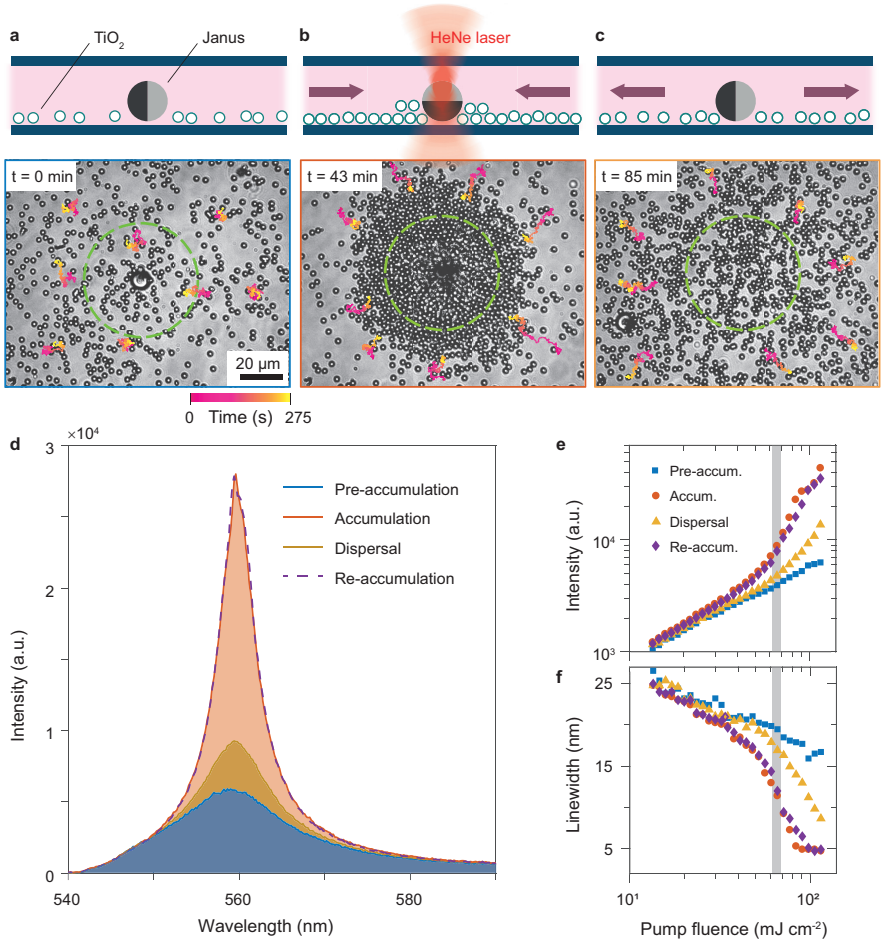

Figure 1: **Reversible self-organisation of colloids in a programmable random laser**. (**a**) A light-absorbing Janus particle in a TiO_2 and laser dye (rhodamine 6G) colloidal dispersion attracts the diffusing colloids (accumulation), which (**b**) assemble in a dense cluster, when illuminated by a HeNe laser (CW, 632.8 nm) (Methods). (**c**) If the HeNe laser is off, the colloids disperse. (**a-c**) A few 275 second-long trajectories highlight the colloids' motion. (**d**) Lasing is observed upon optical pumping (400 ps laser pulses, 532 nm, pump fluence 100 mJ cm^{-2}, dashed area in **a-c**) during accumulation, but not before (pre-accumulation) or after (dispersal). Re-accumulation after dispersal (Fig. E5) confirms lasing recovery. (**e-f**) The spectra show a reversible narrowing of the emission with cluster formation, corresponding to random lasing action, confirmed by (**e**) the nonlinear increase of the peak intensity as a function of pump fluence and (**f**) the reduction of emission linewidth to 5 nm (below threshold at 13.5 nm). The grey-shaded regions show the pump fluence threshold for lasing ($\sim$70 mJ cm^{-2}). A similar narrowing is not observed when the TiO_2 colloids are replaced by colloidal particles of lower refractive index (Fig. E7).

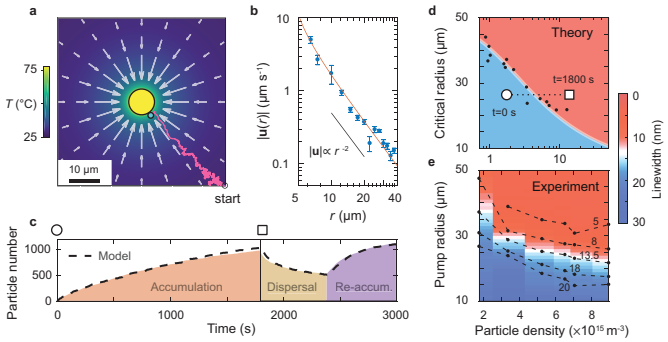

Figure 2: **Dynamics of dissipative colloidal accumulation and random lasing.** (**a**) Calculated temperature profile around a heat source (yellow circle) with the corresponding temperature-induced velocity field (arrows) for a TiO_2 colloid (cyan circle). The over-imposed simulated trajectory (magenta line) shows how motion becomes more directed when approaching the heat source, consistent with (**b**) the experimental (dots) and modelled (line) colloidal radial velocity with distance r from the heat source. The error bars around each data point represent one standard deviation around the mean values. (**c**) Time dynamics of cluster formation (shaded area: experiments; dashed line: simulation) when the heat source is on (accumulation), off (dissipation) and on again (re-accumulation). Time points (circle and square) correspond to start and end of accumulation. (**d-e**) Cluster linewidth versus particle density and pump radius for (**d**) random laser theory and (**e**) experiments with rhodamine 6G (rhodamine B in Fig. E8). The dots highlight experimental values obtained (**d**) at threshold and (**e**) at different linewidths (values in nm in the plot) for different pump radii under a fixed pump fluence (140 mJ cm^{-2}). The circle and square in **d** show the initial and final particle densities around the heat source before and after accumulation (as in **c**). The increase in particle density through accumulation explains the transition from below threshold (blue region) to lasing (red region).

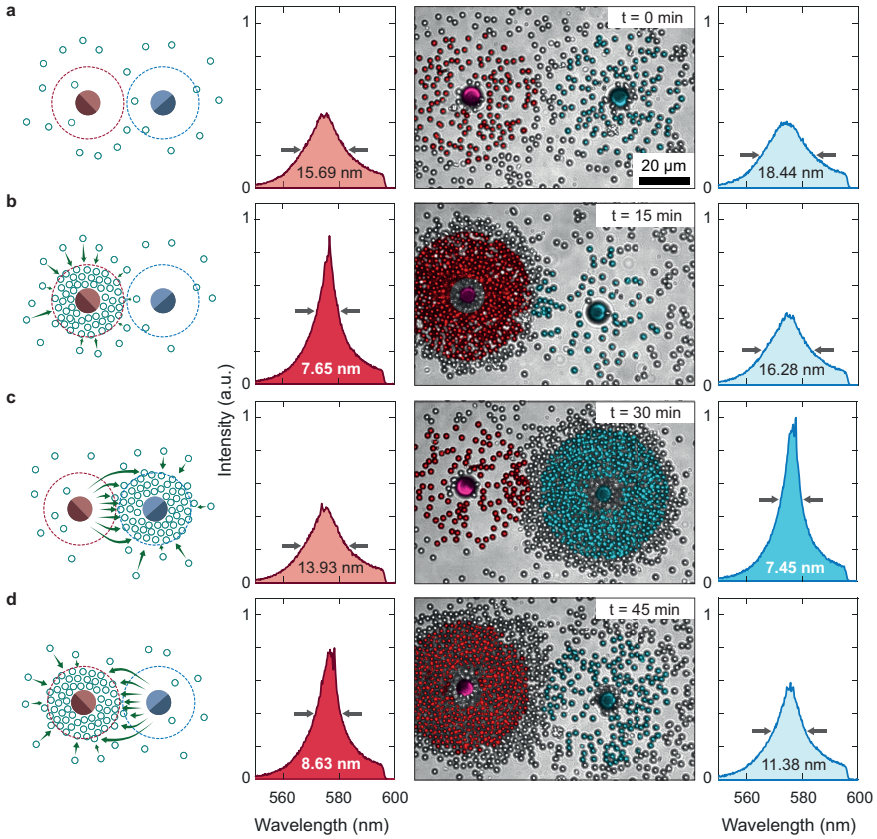

Figure 3: **Reconfiguring random lasers by load transfer.** (**a-d**) Two Janus particles (red and blue) are positioned $\sim$60 μm apart in a TiO_2 and laser dye colloidal solution. The region around each particle is pumped separately with the pump laser at a constant fluence (54 mJ cm^{-2}) for 15 minutes each time. The shaded surrounding colloids highlight the respective pump areas. The side panels show the measured emission spectra and respective linewidths at the end of each accumulation period. (**a**) Before the initial accumulation, lasing is not observed from either region. (**b**) When the left Janus particle is active as heat source, lasing is observed after accumulation. (**c**) The colloidal load can then be transferred to the right Janus particle and (**d**) back by alternating their use as heat sources, thus triggering selective lasing action in a different region at each transfer.

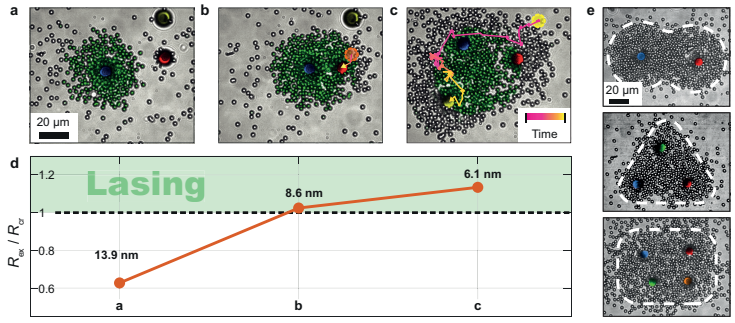

Figure 4: **Cooperative random lasing.** (**a-d**) Multiple Janus particles can act cooperatively to boost lasing action by fusing different colloidal clusters. (**a**) A small cluster of TiO_2 colloids around a single illuminated Janus particle (blue) does not reach the lasing threshold (dashed line in **d**): it has a large linewidth of 13.9 nm and a very low excited system size, $R_{ex}/R_{cr} < 1$ (dots in **d**). (**b**) The cooperative action of a second Janus particle (red) drives the laser just above threshold, (**c**) while the cluster formed with the cooperation of a third particle (yellow) shows an even better lasing action with a small linewidth (6.1 nm) and $R_{ex}/R_{cr} = 1.13$. The trajectories of the second and third Janus particles are highlighted in **b-c**. The green shaded area in **a-c** shows the pump spot size of 52 μm at a fluence of 44 mJ cm^{-2}. (**e**) Three examples of lasing cluster geometries (linewidths of 6.1 nm, 5.7 nm, and 4.7 nm, respectively) achievable when multiple Janus particles cooperate (a hourglass, a triangle, a rectangle), highlighting the structural flexibility of the colloidal assemblies.

References

[1] Whitesides, G. M. & Grzybowski, B. Self-Assembly at All Scales. *Science* **295**, 2418–2421 (2002).

[2] Grzybowski, B. A., Fitzner, K., Paczesny, J. & Granick, S. From Dynamic Self-Assembly to Networked Chemical Systems. *Chem. Soc. Rev.* **46**, 5647–5678 (2017).

[3] Araújo, N. A., *et al.* Steering Self-Organisation through Confinement. *arXiv preprint arXiv:2204.10059* (2022).

[4] Ball, P. Animate materials. *MRS Bulletin* **46**, 553–559 (2021).

[5] Maiti, S., Fortunati, I., Ferrante, C., Scrimin P. & Prins, L. J. Dissipative Self-Assembly of Vesicular Nanoreactors. *Nat. Chem.* **8**, 725–731 (2016).

[6] Bachelard, N., *et al.* Emergence of an Enslaved Phononic Bandgap in a Non-Equilibrium Pseudo-Crystal. *Nat. Mater.* **16**, 808–813 (2017).

[7] Souslov, A., van Zuiden, B. C., Bartolo D. & Vitelli, V. Topological Sound in Active-Liquid Metamaterials. *Nat. Phys.* **13**, 1091–1094 (2017).

[8] Ropp, C., Bachelard, N., Barth, D., Wang, Y. & Zhang, X. Dissipative Self-Organization in Optical Space. *Nat. Photon.* **12**, 739–743 (2018).

[9] Nitta, T., Wang, Y., Du, Z., Morishima, K. & Hiratsuka, Y. A Printable Active Network Actuator Built from an Engineered Biomolecular Motor. *Nat. Mater.* **20**, 1149–1155 (2021).

[10] Palacci, J., Sacanna, S., Steinberg, A. P., Pine, D. J. & Chaikin, P. M. Living Crystals of Light-Activated Colloidal Surfers. *Science* **339**, 936–940 (2013).

[11] Pinçe, E., *et al.* Disorder-Mediated Crowd Control in an Active Matter System. *Nat. Commun.* **7**, 10907 (2016).

[12] Khadka, U., Holubec, V., Yang, H. & Cichos, F. Active Particles Bound by Information Flows. *Nat. Commun.* **9**, 3864 (2018).

[13] Lavergne, F. A., Wendehenne, H., Bäuerle, T. & Bechinger, C. Group Formation and Cohesion of Active Particles with Visual Perception–Dependent Motility. *Science* **364**, 70–74 (2019).

[14] Gao, W., Pei, A., Feng, X., Hennessy, C. & Wang, J. Organized Self-Assembly of Janus Micromotors with Hydrophobic Hemispheres. *J. Am. Chem. Soc.* **135**, 998–1001 (2013).

[15] Wang, W., Duan, W., Sen, A. & Mallouk, T. E. Catalytically Powered Dynamic Assembly of Rod-Shaped Nanomotors and Passive Tracer Particles. *Proc. Natl. Acad. Sci. U.S.A.* **110**, 17744–17749 (2013).

[16] Singh, D. P., Choudhury, U., Fischer, P. & Mark, A. G., Non-Equilibrium Assembly of Light-Activated Colloidal Mixtures. *Adv. Mater.* **29**, 1701328 (2017).

[17] Schmidt, F., Liebchen, B., Löwen, H. & Volpe, G. Light-Controlled Assembly of Active Colloidal Molecules. *J. Chem. Phys.* **150**, 094905 (2019).

[18] Maggi, C., *et al.* Self-Assembly of Micromachining Systems Powered by Janus Micromotors. *Small* **12**, 446–451 (2016).

[19] Yuan, Y., Abuhaimed, G. N., Liu, Q. & Smalyukh, I. I. Self-Assembled Nematic Colloidal Motors Powered by Light. *Nat. Commun.* **9**, 5040 (2018).

[20] Aubret, A., Youssef, M., Sacanna, S. & Palacci, J. Targeted Assembly and Synchronization of Self-Spinning Microgears. *Nat. Phys.* **14**, 1114–1118 (2018).

[21] Vynck, K., *et al.* Light in Correlated Disordered Media. *ArXiv preprint arXiv:2106.13892* (2021).

[22] Goerlitzer, E. S. A., Klupp Taylor, R. N. & Vogel, N. Bioinspired Photonic Pigments from Colloidal Self-Assembly. *Adv. Mater.* **30**, 1706654 (2018).

[23] Sapienza, R. Determining Random Lasing Action. *Nat. Rev. Phys.* **1**, 690–695 (2019).

[24] Wiersma, D. S. The Physics and Applications of Random Lasers. *Nat. Phys.* **4**, 359–367 (2008).

[25] Gottardo, S., *et al.* Resonance-Driven Random Lasing. *Nat. Photonics* **2**, 429–432 (2008).

[26] Lawandy, N. M., Balachandran, R. M., Gomes, A. S. L. & Sauvain, E. Laser Action in Strongly Scattering Media. *Nature* **368**, 436–438 (1994).

[27] Noginov, M. *Solid-State Random Lasers*, vol. 105 (Springer, 2006).

[28] Bachelard, N., Gigan, S., Noblin, X. & Sebbah, P. Adaptive Pumping for Spectral Control of Random Lasers. *Nat. Phys.* **10**, 426–431 (2014).

[29] Luana, F., *et al.* Lasing in Nanocomposite Random Media. *Nano Today* **10**, 168–192 (2015).

[30] Cao, H., Chriki, R., Bittner, S., Friesem, A. A. & Davidson, N. Complex Lasers with Controllable Coherence. *Nat. Rev. Phys.* **1**, 156–168 (2019).

[31] Boschetti, A., *et al.*, Spectral Super-Resolution Spectroscopy Using a Random Laser. *Nat. Photonics* **14**, 177–182 (2020).

[32] Caixeiro, S., Gaio, M., Marelli, B., Omenetto, F. G. & Sapienza, R. Silk-Based Biocompatible Random Lasing. *Adv. Opt. Mater.* **4**, 998–1003 (2016).

[33] Fan, X. & Yun, S.-H. The Potential of Optofluidic Biolasers. *Nat. Methods* **11**, 141–147 (2014).

[34] Shaltout, A. M., Shalaev, V. M. & Brongersma, M. L. Spatiotemporal Light Control with Active Metasurfaces. *Science* **364**, eaat3100 (2019).

[35] Sapienza, R. Controlling Random Lasing Action. *Nat. Phys.* (2022).

[36] Duhr, S. & Braun, D. Two-Dimensional Colloidal Crystals Formed by Thermophoresis and Convection. *Appl. Phys. Lett.* **86**, 131921 (2005).

[37] Piazza, R. & Parola, A. Thermophoresis in Colloidal Suspensions. *J. Phys. Condens. Matter* **20**, 153102 (2008).

[38] Lin, L., *et al.*, Opto-Thermophoretic Assembly of Colloidal Matter. *Sci. Adv.* **3**, e1700458 (2017).

[39] Sharma, V., Paul, D., Chaubey, S. K., Tiwari, S. & Kumar, G. P. Large-Scale Optothermal Assembly of Colloids Mediated by a Gold Microplate. *J.Phys. Condens. Matter* **32**, 324002 (2020).

[40] Ciraulo, B., Garcia-Guirado, J., de Miguel, I., Arroyo, J. O. & Quidant, R. Long-Range Optofluidic Control with Plasmon Heating. *Nat. Commun.* **12**, 2001 (2021).

[41] Fränzl, M. & Cichos, F. Hydrodynamic Manipulation of Nano-Objects by Optically Induced Thermo-Osmotic Flows. *Nat. Commun.* **13**, 656 (2022).

[42] Lin, L., Hill, E. H., Peng, X. & Zheng, Y. Optothermal Manipulations of Colloidal Particles and Living Cells. *Acc. Chem. Res.* **51**, 1465–1474 (2018).

[43] Makey, G., *et al.*, Universality of Dissipative Self-Assembly from Quantum Dots to Human Cells. *Nat. Phys.* **16**, 795–801 (2020).

[44] Prizia, R., Conti, C. & Ghofraniha, N. Soret Reverse Saturable Absorption of Graphene Oxide and its Application in Random Lasers. *J. Opt. Soc. Am. B* **36**, 19–25 (2019).

[45] Kim, Y. Shah, A. A. & Solomon, M. J. Spatially and Temporally Reconfigurable Assembly of Colloidal Crystals. *Nat. Commun.* **5**, 3676 (2014).

[46] Yan, J., *et al.*, Reconfiguring Active Particles by Electrostatic Imbalance. *Nat. Mater.* **15**, 1095–1099 (2016).

[47] Gaio, M., Caixeiro, S., Marelli, B., Omenetto, F. G. & Sapienza, R. Gain-Based Mechanism for p H Sensing Based on Random Lasing. *Phys. Rev. Applied* **7**, 034005 (2017).

[48] Phillips, C. L., *et al.*, Digital Colloids: Reconfigurable Clusters as High Information Density Elements. *Soft Matter* **10**, 7468–7479 (2014).

[49] Kim, S.-H., Lee, S. Y., Yang, S.-M. & Yi, G.-R. Self-Assembled Colloidal Structures for Photonics *NPG Asia Mater.* **3**, 25–33 (2011).

Methods

Materials

Glass microscopy slides (Thermo Fisher) were purchased from VWR while glass coverslips were purchased from Thorlabs. The following chemicals were purchased and used as received: rhodamine 6G (Sigma-Aldrich), rhodamine B (Acros Organics), acetone ($\geq$ 99.8%, Sigma-Aldrich), ethanol ($\geq$ 99.8%, Fisher Scientific), sodium hydroxide (NaOH, Fisher Scientific), polyethylenimine (PEI, branched, Mw 25,000, Mn 10,000, Sigma-Aldrich). Deionised (DI) water ($\geq$ 18 MΩ.cm) was collected from a Milli-Q purification system. Aqueous colloidal dispersions (5% w/v) of silica (SiO_2) colloids for fabricating Janus particles and to be used as spacers (8.44 $\pm$ 0.27 μm and 20 ± 0.64 μm in diameter, respectively) were purchased from Microparticles GmbH. Aqueous colloidal dispersions of titania (TiO_2) particles (2.5% w/v, 1.73 ± 0.03 μm in diameter) for the lasing experiments, of fluorescent SiO_2 particles (2.5% w/v, 10.05 $\pm$ 0.31 μm, excitation/emission: 602 nm/623 nm) for Fig. E4 and of polystyrene particles (10% w/v, 1.65 $\pm$ 0.04 μm) for Fig. E7 were also purchased from Microparticles GmbH. Carbon rods of length 300 mm and diameter 6.15 mm for coating Janus particles were purchased from Agar Scientific and cut to a length of 50 mm before use. UV cure adhesive (Blufixx) and hydrophobic coating (RainX) for sample preparation were purchased from an online retailer (Amazon).

Slide cleaning protocol

Before their use for sample preparation, glass slides and coverslips were cleaned via sonication for 10 min in 2 M NaOH ethanolic solution followed by three cycles of 5 min sonication in DI water. To dry them, the slides were withdrawn from the water in the presence of ethanol vapor (Marangoni drying) and, subsequently, blown with a nitrogen gun.

Fabrication of Janus particles

The Janus particles used in our experiments as heat sources were fabricated from $\mathrm{SiO_2}$ colloids of radius $R_\mathrm{s} = 4.22 \pm 0.14\,\mu\mathrm{m}$, which were coated on one side with a thin layer ($\approx 60\,\mathrm{nm}$) of carbon. We first deposited a monolayer of colloids on a clean glass slide. The monolayer was obtained by evaporating a $40\,\mu\mathrm{L}$ droplet containing a $2.5\%\,\mathrm{w/v}$ dispersion of the colloids in DI water. The particles were then coated with a 60 nm thick carbon layer using an automatic carbon coater (AGB7367A, Agar Scientific). Post-coating sonication allowed us to dislodge the half-coated particles in DI water from the glass slides to use them for sample preparation. Due to their micrometric size, the use of Janus particles as heat sources eased their visualisation, characterisation and manipulation in crowded colloidal environments. The ability to easily identify the heat sources was key for tracking them in Figs. 3 and 4 and for measuring the induced local temperature increase as a function of laser power in Fig. E6.

Preparation of samples of colloids and laser dyes

Random lasers combine optical gain with a scattering medium [23]. The samples used are in the form of a glass chamber (see next section) filled with a colloidal dispersion in an ethanol solution of laser dye. The optical gain is provided by two types of rhodamine-based dyes in ethanol solution (1% w/v): rhodamine 6G (Rh6G) for Figs. 1, 2, E5 and E7, and rhodamine B (RhB) for Figs. 3, 4 and E8. The use of the two dyes is motivated by their complementary features in experiments: at $\lambda = 532$ nm (the wavelength of the pump laser), pumping rhodamine 6G (absorption peak at 530 nm) is more efficient than pumping rhodamine B (absorption peak at $\lambda = 550$ nm), thus improving lasing performance at a given power (i.e. narrower linewidth); RhB solutions instead reduce sticking of Janus particles to the glass substrate, thus performing better for tasks where their manoeuvrability is paramount. The scattering medium is a dispersion of monodisperse $\mathrm{TiO_2}$ colloids, chosen due to the material's characteristic high refractive index ($n_{\mathrm{TiO_2}} \approx 2.3$ for amorphous titania) larger than that of ethanol ($n_{EtOH} = 1.36$). This refractive index difference is important to achieve the strong scattering properties needed for lasing action: in fact, no lasing is observed when substituting the $\mathrm{TiO_2}$ colloids with lower refractive index polymer colloids of similar size (Fig. E7) [25]. We obtained stable dispersions of $\mathrm{TiO_2}$ colloids in 1% w/v ethanol solutions of laser dyes (either rhodamine 6G or rhodamine B) by functionalising the colloids with PEI to prevent flocculation and sticking to the glass substrate [50]. In particular, we first mixed $50\,\mu\mathrm{L}$ of a 0.1% aqueous dispersion of Janus particles with stock solutions of $\mathrm{TiO_2}$ colloids ($20\,\mu\mathrm{L}$) and $20\,\mu\mathrm{m}$ $\mathrm{SiO_2}$ colloids ($10\,\mu\mathrm{L}$) in a 1.5 mL centrifuge tube (Eppendorf). The $20\,\mu\mathrm{m}$ $\mathrm{SiO_2}$ colloids were added to act as spacers in the sample chambers. This colloidal cocktail is then centrifuged at 1000 RCF for 3 min leaving a pellet; the supernatant is removed and the pellet is redispersed in $100\,\mu\mathrm{L}$ of a 3% w/v ethanol solution of PEI. The dispersion is then sonicated for 5 min to fully redisperse the $\mathrm{TiO_2}$ colloids and to allow for functionalising their surface with PEI, as confirmed by Fourier-transform infrared spectroscopy (FTIR) in Fig. E2. After functionalisation with PEI, the size of the $\mathrm{TiO_2}$ colloids

increased to 1.83 ± 0.05 μm from 1.73 ± 0.03 μm of the pristine particles as confirmed by scanning electron microscopy measurements. The dispersion is left to rest for 30 min to make sure all particles are sufficiently coated with the polymer. Finally, it is centrifuged again at 1000 RCF for 2 min, the supernatant removed and replaced with $50\,\mu$L of a 1% w/v ethanol solution of a rhodamine dye.

Sample chamber preparation

Experiment-ready sample chambers containing a dispersion of colloids in ethanol solutions of laser dyes were prepared by sandwiching $15\,\mu$L of the dispersion between a clean glass slide and a thin coverslip using low concentrations of $20\,\mu$m silica particles as spacers. Prior to this, both slide and coverslip were soaked for 2 min in Rain-X, a commercial solution which renders glass surfaces more hydrophobic and aids limiting particle sticking to the glass chamber. Excess RainX was removed by soaking the slide in acetone and subsequently wiping with lens tissue. The chamber was then sealed by applying a UV curable adhesive around the borders of the coverslip, taking care of not exposing the dye solution to UV light by illuminating only the edges of the coverslip, as this could cause dye bleaching. Before data acquisition, the sample was left to equilibrate over a one-hour period.

Optical setup and microscopy

Fig. E3 shows a schematic of the experimental setup used to illuminate the Janus particles, to image the sample and to probe its emission spectra. Samples are mounted on the stage of a Nikon Ti microscope. Two laser sources are exploited: a continuous-wave HeNe laser (Thorlabs, $\lambda = 632.8$ nm, CW, 20 mW) and a Nd:YAG pulsed laser (TEEM Power-Chip, $\lambda = 532$ nm, pulse width 400 ps, 20 μJ energy per pulse, 1-1000 Hz). The HeNe laser is used as a energy source for heating the Janus particles, while the pulsed laser is used to reach population inversion for lasing measurements. The choice of using the HeNe as energy source was dictated by the need to avoid overlap with the absorption spectrum of rhodamine dyes (centred at 525 nm), thus avoiding spurious heating effects in the sample due to this competing absorption process in the dye. The pulsed laser is only operating when measuring emission spectra and in single shot mode for less than 30 s each time to limit absorption from the Janus particle and to avoid modification of the accumulated colloidal cluster.

The HeNe laser is coupled to a single-mode optical fibre and the beam from the fibre is focused onto the sample with a lens of 60 mm focal length to a spot diameter of ~ 5 μm. This spot size was chosen to match the size of the Janus particle and for ease of alignment while making sure the Janus particle is heated with sufficient power density. For accumulation of TiO_2 colloids around the Janus particle to occur, the laser power density at the sample was around 0.14 mW $\mu\mathrm{m}^{-2}$. The laser power was controlled by a movable knife edge before the fibre-coupler. The same HeNe laser was also used to manipulate the Janus particles by optical forces or cavitation (see next section).

For lasing measurements, samples were optically pumped at room-temperature with the Nd:YAG pump laser. The pump laser profile was shaped with a programmable digital micro-mirror device (DMD, Ajile AJD-4500), and the excitation pattern was imaged onto the sample through a 40× objective lens (Nikon CFI Plan Fluor 40X, 0.75 N.A., 0.66 mm W.D.). An acousto-optic modulator (AOM) is used to control the energy of the pump laser. Circular illumination profiles, of constant intensity in a disk shape, and radius $R_{\mathbf{ex}}$, were used for the measurements in Figs. 1, 2, 4, E5 and E8. Doughnut-shaped profiles, of constant intensity in a disk shape without the central part, centred on the Janus particle were used for Fig. 3 and E7 to avoid further laser exposure and prevent any motion of the Janus particle. The size of the missing central part was chosen to be about 1.5 times bigger than the size of the Janus particle for ease of alignment. When the sample was pumped, the HeNe laser was blocked to avoid overheating the Janus particle, and in particular to minimise the formation of cavitation bubbles during the lasing measurements. The lasing emission from the sample was collected through the same objective lens, filtered, and then focused into a stripe on the spectrometer entrance slit via a cylindrical lens to maximise the measured signal counts. The signal was spectrally analysed using a grating spectrometer (Princeton Instruments Isoplane-320) equipped with a 600 gr mm^{-1} visible grating (0.5 nm resolution) and a CCD camera (Princeton Instruments Pixis 400). Linewidths are given as full width at half maximum (FWHM). Fluctuations in the recorded spectra are caused by the dynamic colloidal system as well as by the small fluctuations (around 3%) of the pump laser pulse energy. Overall, the variation of the intensity peak of the random lasing spectra is of approximately 6.4%, which is the standard deviation obtained from a 6 minute-long measurement.

The critical radius $R_{\mathbf{cr}}$ in Fig. 2 was measured at constant pump fluence of 140 mJ cm^{-2}, by changing the size of the illumination spot of radius $R_{\mathbf{ex}}$ while recording the emission spectrum, until the emission linewidth reached the value of 13.5 nm, which is half the fluorescence linewidth measured at low pumping powers.

The motion of the $\mathrm{TiO_2}$ colloids in Figs. 1, 2 and E5 was recorded using a CMOS camera (Thorlabs) at a frame rate of 2 fps (frames per second). Image focus was adjusted so that each particle had a bright spot at its centre relative to the background to provide enough contrast to discern individual particles via digital video microscopy based on a homemade MATLAB tracking software [51].

Manipulation of Janus particle

In order to position the Janus particles at different locations in the sample chamber, we manipulated them with the mildly focused HeNe laser, which, at power densities of 0.14 mW μm^{-2}, exerts a gentle pulling optical force which predominantly drags the Janus particle towards the centre of the laser spot. The manipulation was performed by either moving the sample stage only (Figs. 1, 2, 3, E5 and E7) or the HeNe laser spot only (Fig. 4), while keeping the other element fixed. The same HeNe laser at higher power densities (above 0.2 mW μm^{-2}) was also used to free the Janus particles in $\mathrm{TiO_2}$ clusters by cavitation before repositioning them (Figs.

3 and 4). Cavitation is created when the Janus particle is strongly heated by the HeNe laser leading to bubble formation (Fig. E6) and provides an instantaneous pushing action against the carbon-side of the Janus particle that propels it away from the surrounding $\mathrm{TiO_2}$ colloids.

Calculation of the temperature profile around a heat source

As the dynamics of our dissipative colloidal assemblies around an illuminated Janus particle predominantly take place near the glass surface, we can calculate the temperature profile generated by a disc heat source of radius R_s at temperature T_s in two dimensions. This is a reasonable approximation considering that the most likely configuration for the Janus particle in a formed cluster is with the cap facing down, i.e. towards the interface (Fig. E4). Under continuous illumination, the heating of the surrounding fluid can be assumed instantaneous so that a steady-state temperature profile around the heat source is promptly reached. In fact, since heat propagation is much faster than particle migration, the temperature field can be considered as stationary. Assuming a steady state for the diffusion of heat from the source, we can then calculate the temperature profile around the heat source in the plane of motion as [52]:

$$T(r) = \frac{2}{\pi}(T_\mathrm{s} - T_\mathrm{b}) \sin^{-1}\left(\frac{R_\mathrm{s}}{r}\right) + T_\mathrm{b}, \text{ for } r \geq R_\mathrm{s} \tag{2}$$

where r is the radial distance from the centre of the heat source and T_b is room temperature. Note that, in steady state, the presence of an interface does not influence the temperature profile.

Particle-based simulations

We consider a simple numerical model where N hard spheres of mean radius $R_{\mathrm{TiO_2}}$ move inside a two-dimensional square box of side $B = 187\,\mu\mathrm{m}$. Particles were placed at random without overlap at fixed density (0.0425 particles $\mu\mathrm{m}^{-2}$). Otherwise specified differently, the values for all parameters in the simulations are set to the exact experimental values reported in the main text. The radius of each individual particle R_i is taken from a Gaussian distribution with mean $R_{\mathrm{TiO_2}}$ and standard deviation δR to reproduce the size variability of the monodisperse sample of $\mathrm{TiO_2}$ colloids. At the centre of the box, we place a disc heat source of radius R_s. When the source is active, it has a uniform temperature T_s and generates a radial temperature profile according to Eq. 2. When the source is not active, the temperature is uniform in the box and equivalent to room temperature T_b.

The trajectory of the i-th particle is then obtained by solving the following Langevin equation in the overdamped regime using the second-order stochastic Runge-Kutta numerical scheme [53]

$$\dot{\mathbf{x}}_i = \mathbf{u}_i + \sum_{j \neq i} \frac{\mathbf{F}_{ji}}{\gamma_i} + \frac{\mathbf{F}_{\mathrm{s}i}}{\gamma_i} + \sqrt{2D_i}\boldsymbol{\xi}_i, \tag{3}$$

where $\mathbf{x}_i$ and $\mathbf{u}_i$ are respectively the particle's position and temperature-induced drift velocity at time t (Eq. 1), $D_i = k_\mathrm{B}T_i/\gamma_i$ is the particle's diffusion coefficient at position $\mathbf{x}_i$ and temperature T_i (Eq. 2) with γ_i its friction coefficient [54]; $\boldsymbol{\xi}_i$ is a two-dimensional vector of independent white noise process with zero mean and unitary variance [54]. When the heat source is off, $\mathbf{u}_i$ is null. The direction of motion due to the temperature-induced drift velocity is therefore defined by the unitary vector $\hat{\mathbf{e}}_r^i(t) = [\cos(\theta_i(t)),\, \sin(\theta_i(t)]$, where $\theta_i(t)$ is the particle's angular coordinate in the frame of reference defined by the heat source.

We implemented particle-particle steric interactions $\mathbf{F}_{ji}$ with the repulsive term of a Lennard-Jones potential with parameters $\epsilon = k_\mathrm{B}T_\mathrm{b}$ and $\sigma = 2R_{\mathrm{TiO}_2}$. The effect of this repulsive term is short ranged and was truncated at $1.6(R_i + R_j)$ for each neighbouring particles i and j. Finally, we modelled the steric interaction with the heat source by introducing a repulsive force $\mathbf{F}_{si}(r_i)$ in the equation of motion. This force depends on the particle's distance $\mathbf{r}_i$ from the heat source as

$$\mathbf{F}_{si}(r_i) \propto \frac{e^{-r_i}}{|r_i - R_s + R_i|}\hat{\mathbf{e}}_r^i. \tag{4}$$

This function was chosen to reproduce a strong (local) repulsive interaction between particle and source, i.e. to mimic a hardcore potential. The exponential term ensures that the force does not increase too abruptly when approaching the source. This effect of this force was truncated at a cut-off distance $r_\mathrm{c} = 2.5R_\mathrm{s}$.

Random lasing model

The random lasing model is based on the radiative transfer equation (RTE) [55] and estimates the critical radius R_cr, which is the minimum size of a colloidal cluster needed to achieve the lasing threshold. Since the lateral dimensions of our sample are much larger than its thickness, we used a two-dimensional model where R_cr is given by solving

$$\frac{J_0(\sqrt{2g(\ell_\mathrm{sc}^{-1} - g)}R_\mathrm{cr})}{J_1(\sqrt{2g(\ell_\mathrm{sc}^{-1} - g)}R_\mathrm{cr})} = \frac{\pi}{2}\frac{g}{\sqrt{2g(\ell_\mathrm{sc}^{-1} - g)}}, \tag{5}$$

where J_0 and J_1 are the Bessel functions of the first kind, $\ell_\mathrm{sc} = 1/(\sigma_\mathrm{sc}\rho)$ is the scattering length (σ_sc is the scattering cross-section and ρ is the particle density), and $g = 1/\ell_\mathrm{g,dye}$ is the gain coefficient of the gain medium, being $\ell_\mathrm{g,dye}$ the dye gain length. In our self-organised lasers, ℓ_sc and hence R_cr depend on the time-varying particle density in the accumulation/dispersal processes.

In order to find the critical radii of the clusters with different particle densities at different times, Eq. 5 was solved numerically, with g a fitting parameter and ℓ_sc obtained from Mie theory for TiO_2 colloids of 1.83 μm diameter and a refractive index $n_{\mathrm{TiO}_2} = 2.3$. We chose to fit g as its exact value depends on off-plane scattering losses (i.e. when light escapes from the sample plane) and on minor absorption losses from the partially pumped dye and the Janus particle, and

therefore it is usually larger than $\ell_{\mathrm{g,dye}}$. A good fit to the experimental data in Fig. 2d is obtained with $g_{\mathrm{net}} = 0.0721\,\mu\mathrm{m}^{-1}$ (corresponding to a net dye gain length $\ell_{\mathrm{g,net}} = 13.87\,\mu\mathrm{m}$). This gain length estimate is around 3.5 times larger than $\ell_{\mathrm{g,dye}} = 4\ \mu$m given that, for rhodamine, $\sigma_{\mathrm{g,dye}} = 2 \times 10^{-20}\ \mathrm{m}^2$ [56] and that the dye density $\rho_{\mathrm{dye}} = 1.257 \times 10^{25}\,\mathrm{molecules\,m}^{-3}$ in a 1% w/v ethanol solution (the molar mass of rhodamine is 479 g mol^{-1}).

The value of ℓ_{sc} (as estimated from Mie scattering calculations and particle counting from bright-field images) reaches a minimum value of 13 μm for a dense cluster, much larger than the light wavelength, while for a dilute cluster is of the order of 100 μm. The optical thickness, i.e. the cluster diameter divided by ℓ_{sc}, is smaller than 6. This justifies our modelling of the random laser in the intermediate regime between the diffusive and ballistic limits [55]

Data availability.

Source data are available for this paper in figshare with the digital object identifier 10.6084/m9.figshare.19745293 (https://doi.org/10.6084/m9.figshare.19745293) [57]. All other data that support the plots within this paper and other findings of this study are available from the corresponding author upon reasonable request.

Code availability.

The code that supports the findings of this study is available from the corresponding authors upon reasonable request.

References

[50] Tang, F., Uchikoshi, T., Ozawa, K. & Sakka, Y. Effect of Polyethylenimine on the Dispersion and Electrophoretic Deposition of Nano-Sized Titania Aqueous Suspensions. *J. Eur. Ceram. Soc.* **26**, 1555–1560 (2006).

[51] Crocker, J. C. & Grier, D. G. Methods of Digital Video Microscopy for Colloidal Studies. *J. Colloid Interf. Sci.* **179**, 298–310 (1996).

[52] Warrick, A., Broadbridge, P. & Lomen, D. Approximations for Diffusion from a Disc Source. *Appl. Math. Model.* **16**, 155–161 (1992).

[53] Brańka, A. C. & Heyes, D. M. Algorithms for Brownian Dynamics Computer Simulations: Multivariable Case. *Phys. Rev. E* **60**, 2381 (1999).

[54] Volpe, G., Gigan, S. & Volpe, G. Simulation of the Active Brownian Motion of a Microswimmer. *Am. J. Phys.* **82**, 659–664 (2014).

[55] Guerin, W., *et al.* Diffusive to Quasi-Ballistic Random Laser: Incoherent and Coherent Models *J. Opt. Soc. Am. B* **33**, 1888–1896 (2016).

[56] Holzer, W., *et al.* Photo-Physical Characterization of Rhodamine 6G in a 2-Hydroxyethyl-Methacrylate Methyl-Methacrylate Copolymer. *Chem. Phys.* **256**, 125–136 (2000).

[57] Trivedi, M., Saxena, D., Ng, K. W., Sapienza, R. & Volpe, G. Dataset for Self-organised Lasers of Reconfigurable Colloidal Assemblies. *Figshare*, https://doi.org/10.6084/m9.figshare.19745293 (2022).